

A nonprotein thermal hysteresis-producing xylomannan antifreeze in the freeze-tolerant Alaskan beetle *Upis ceramboides*

Kent R. Walters, Jr.^{a,1}, Anthony S. Serianni^b, Todd Sformo^c, Brian M. Barnes^c, and John G. Duman^a

^aDepartment of Biological Sciences and ^bDepartment of Chemistry and Biochemistry, University of Notre Dame, Notre Dame, IN 46556; and ^cInstitute of Arctic Biology, University of Alaska Fairbanks, Fairbanks, AK 99775

Edited by George N. Somero, Stanford University, Pacific Grove, CA, and approved October 13, 2009 (received for review September 1, 2009)

Thermal hysteresis (TH), a difference between the melting and freezing points of a solution that is indicative of the presence of large-molecular-mass antifreezes (e.g., antifreeze proteins), has been described in animals, plants, bacteria, and fungi. Although all previously described TH-producing biomolecules are proteins, most thermal hysteresis factors (THFs) have not yet been structurally characterized, and none have been characterized from a freeze-tolerant animal. We isolated a highly active THF from the freeze-tolerant beetle, *Upis ceramboides*, by means of ice affinity. Amino acid chromatographic analysis, polyacrylamide gel electrophoresis, UV-Vis spectrophotometry, and NMR spectroscopy indicated that the THF contained little or no protein, yet it produced 3.7 ± 0.3 °C of TH at 5 mg/ml, comparable to that of the most active insect antifreeze proteins. Compositional and structural analyses indicated that this antifreeze contains a β -mannopyranosyl-(1 \rightarrow 4) β -xylopyranose backbone and a fatty acid component, although the lipid may not be covalently linked to the saccharide. Consistent with the proposed structure, treatment with *endo*- β -(1 \rightarrow 4)xylanase ablated TH activity. This xylomannan is the first TH-producing antifreeze isolated from a freeze-tolerant animal and the first in a new class of highly active THFs that contain little or no protein.

antifreeze protein | freeze tolerance | insect cold tolerance | thermal hysteresis | xylomannan

Antifreeze proteins and glycoproteins (AF(G)Ps) were first identified in the blood of Antarctic fishes, in which they allow these fish to avoid freezing in ice-laden waters that are colder than the colligative melting point of their bodily fluids (1). AF(G)Ps adsorb to the surface of ice and prevent water from joining the crystal lattice, thereby preventing freezing of a solution in the presence of ice until a new, lower (hysteretic) freezing point is reached (1, 2). Thermal hysteresis (TH), defined as the difference between the colligative melting and hysteretic freezing points, is diagnostic for the presence of large-molecular-mass antifreezes such as AF(G)Ps.

Since their discovery, AF(G)Ps have been the subjects of active research, ranging from structural biochemistry (1) to ecological physiology (3) and applications in biotechnology (4). This body of work has revealed the existence of five distinct structural classes of fish AF(G)Ps (5) and has demonstrated some unexpected functions of these proteins. In addition to producing TH, all AF(G)Ps appear to prevent the recrystallization of ice (6), and certain fish AF(G)Ps may protect cell membranes from low-temperature-induced injury (7, 8).

More recently, TH has been described in additional taxa, representing four kingdoms of life (1, 2, 9–11). Structurally distinct AF(G)Ps have been isolated and characterized from plants, insects, collembola, fungi, and bacteria (6, 12–15), showing that diverse proteins with TH activity have evolved in distantly related cold-tolerant organisms. However, the majority of the responsible thermal hysteresis factors (THFs) have not been isolated or structurally characterized (i.e., chemical composition has not been determined). In insects, for instance, TH

has been identified in more than 50 species (9), but antifreeze protein (AFP) sequences have been published for only four of these (4). Furthermore, TH has been observed in multiple species of freeze-tolerant insects (9, 16, 17), namely, those able to survive extracellular freezing; however, none of the responsible THFs have been structurally characterized.

Although the structures of known THFs are extremely diverse and appear to have evolved independently multiple times even within closely related taxa (18), proteins were the only biomolecules previously known to produce TH. The xylomannan described herein is the first THF isolated from a freeze-tolerant animal and the first containing little or no protein.

Results and Discussion

THF Isolated from *U. ceramboides* Is Highly Active and Contains Little or No Protein. We investigated the THFs in adult darkling beetles, *U. ceramboides*, from interior Alaska because they tolerate freezing to -60 °C in midwinter (19) and were reported to exhibit ≈ 0.4 °C of TH in their hemolymph after cold acclimation (9). We typically observed TH values < 0.1 °C and often detected only hexagonal ice crystal morphology in the hemolymph of cold-adapted insects, indicating the presence of a low concentration of THF and/or a low specific activity THF (6). The sporadic presence of > 0.5 °C of TH in the hemolymph of *U. ceramboides* is consistent with observations on other freeze-tolerant arthropods (16, 20).

To isolate the THF, we homogenized 40.3 g of cold-acclimated *U. ceramboides* and solubilized molecules of increasing membrane affinity in three successive extractions. THFs present in each extract (R1, soluble fraction; R2, first membrane-associated fraction; R3, second membrane-associated fraction) were separated from other solutes by ice affinity (21). The isolated THFs in the R1, R2, and R3 fractions weighed ≈ 125 μ g, ≈ 100 μ g, and ≈ 60 μ g, respectively, and exhibited $\approx 3.7 \pm 0.3$ °C of TH at 5 mg/ml, a value comparable to that of the most active insect antifreeze proteins (12).

THFs (2–5 μ g) from each extraction was analyzed by PAGE. The THFs migrated toward the anode on both native and denaturing gels (Fig. 1 C) but could not be visualized with Coomassie, silver, or SYPRO Ruby protein stains (Fig. 1), even though the detection limits of the three assays are 2 to 3 orders of magnitude lower than the amount of THF applied to the gel (22). These findings suggested that the isolated THF contained little or no protein. One faint protein band (≈ 80 kDa) was detected in the R1 fraction (Fig. 1), but no corresponding band was observed in R2, suggesting that an “ice-active” protein was present in the soluble fraction. Certain non-THF ice-active

Author contributions: K.R.W., A.S.S., and J.G.D. designed research; K.R.W., T.S., and B.M.B. performed research; K.R.W., A.S.S., and J.G.D. analyzed data; and K.R.W. wrote the paper.

The authors declare no conflict of interest.

This article is a PNAS Direct Submission.

¹To whom correspondence should be addressed. E-mail: kwalter2@nd.edu.

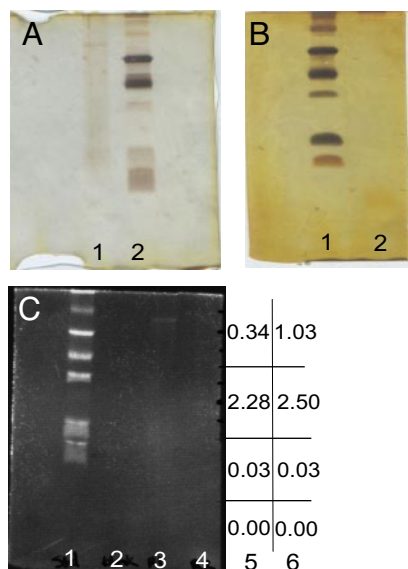


Fig. 1. SDS/PAGE (12%) of R1 and R2 fractions. (A) Silver-stained gel. Lane assignments: 1, ice-purified R1; 2, low-molecular-weight standards. (B) Silver stained gel. Lane assignments: 1, low-molecular-weight standards; 2, ice purified R2. (C) Gel stained with Sypro Ruby. Lane assignments: 1, low molecular weight standards; 2, blank (loading dye only); 3, ice purified R1; 4, ice purified R2. Ice-purified R1 and R2 were applied to two additional lanes (lanes 5 and 6, respectively), which were excised from the gel. Each lane was divided into four segments and the THF was eluted in distilled water overnight. After dialysis, the sample was concentrated and TH was measured. TH values ($^{\circ}\text{C}$) are shown for lanes 5 and 6 for each gel fragment.

molecules, such as ice nucleating proteins, are likely components of the hemolymph of *U. ceramoides* (23) and may be isolated by ice affinity (24). Furthermore, membrane filtration (30,000 MW cut-off) concentrated the ≈ 80 kDa R1 protein in the retentate, whereas TH was observed only in the filtrate. Treatment of the isolated THF with Pronase had no effect on TH activity, further supporting the absence of a protein scaffold.

Ancillary spectrophotometric characterization of the THFs also supports the absence of a significant protein component. Maximal UV absorbance of the THF occurred below 200 nm (Fig. 2); maximal absorbance is expected at 205–220 nm for peptide bonds. In addition, there was no absorbance peak near 280 nm, suggesting the absence of aromatic amino acids. ^1H NMR spectra also lacked any major signals that supported the presence of protein, as all major signals appeared to arise from saccharide and lipid constituents (Fig. 3). Furthermore, ^1H NMR spectra lacked downfield resonances characteristic of

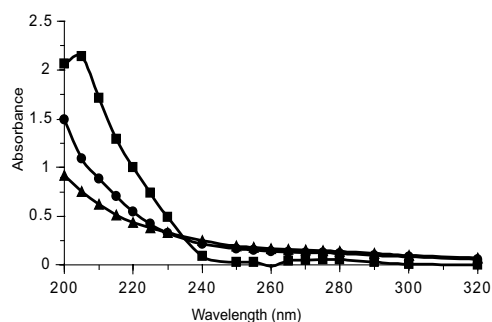


Fig. 2. UV absorbance spectra of R1 and R2 fractions compared with that of BSA. Squares, BSA at 0.12 mg/ml; circles, 1:100 dilution of R2; triangles, 1:100 dilution of R1.

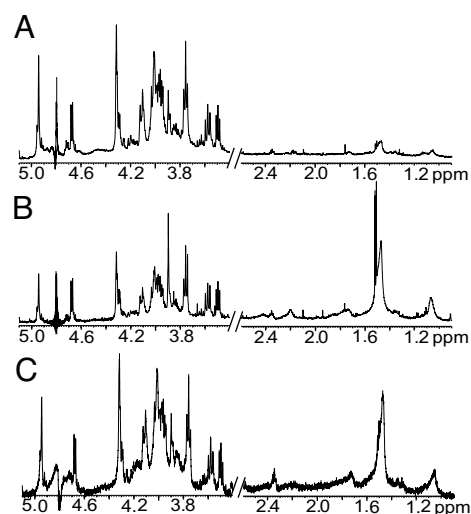


Fig. 3. A comparison of 600 MHz ^1H NMR spectra of THFs isolated by ice affinity from three successive extraction buffers. (A) Buffer R1, soluble fraction. (B) Buffer R2, first membrane-associated fraction. (C) Buffer R3, second membrane-associated fraction. Decreasing signal to noise indicates lower THF concentrations.

aromatic protons. Although a single, low-intensity signal at 8.65 ppm was observed in the R1 and R2 fractions (for R3, spectral signal/noise was not sufficient to permit observation of this signal). However, this singlet is not consistent with the presence of aromatic amino acids, inasmuch as these give rise to multiple aromatic proton signals. Amino acid chromatographic analysis revealed that the ice-purified sample contained 2–3% amino acid by mass, most likely contributed by contaminating proteins/amino acids or a minor protein component in the THF.

THF Comprises a Xylopyranose–Mannopyranose Core and Possibly a Lipid Component. Qualitatively, ^1H NMR spectra of the R1, R2, and R3 fractions were nearly identical, each containing the same major signals attributable to saccharide and fatty acid components (Fig. 3) based on their characteristic chemical shifts. Inspection of the ^1H and ^{13}C chemical shifts, ^1H – ^1H scalar couplings ($^3J_{\text{H}_2,\text{H}_3}$), signal multiplicities (Table 1), and relative signal areas of the $-\text{CH}_2-$ and $-\text{CH}_3$ signals observed in the ^1H NMR spectrum of R1 (Fig. 4) indicate the presence of a saturated fatty acid. 2D ^1H – ^1H total correlation spectroscopy (TOCSY) data showed that the putative fatty acid signals in R1 arise from a single spin system (Fig. 4). The ^1H NMR spectrum of R2 contained two additional broad signals, observed at 5.5 ppm ($-\text{HC}=\text{CH}-$) and 2.2 ppm ($-\text{H}_2\text{C}=\text{HC}=\text{CH}-\text{CH}_2-$), suggesting the presence of unsaturated fatty acid in this sample (25).

There were notable quantitative differences between the spectra. ^1H NMR spectra of the membrane-extracted fractions, R2 and R3, contained considerably more intense lipid signals than did that of the soluble R1 fraction (Fig. 3), indicating a greater fatty acid component in R2 and R3, which suggests that the fatty acid component may anchor the THF to the cell membrane. However, the mode of lipid linkage to the saccharide has not been established, and it remains possible that the lipid is not covalently linked to the saccharide constituent.

Methanolysis of R1 followed by tandem GC/MS analysis of derivatized monosaccharides showed that the two predominant monosaccharides in the R1 sample were mannose (Man) and xylose (Xyl). These results are consistent with the characteristics of the anomeric ^1H signals observed in the ^1H NMR spectrum based on signal intensities and splittings (Fig. 3). The $\approx 1.3:1$ Man:Xyl molar ratio determined by integration of the anomeric

Table 1. ^{13}C and ^1H chemical shifts (ppm) and ^1H - ^1H spin-couplings for lipid signals in R1 compared with those observed for a glycolipid isolated from *Deinococcus radiodurans*

	Chemical shifts (ppm)				J -coupling (Hz)
	CH_2CO	$\text{CH}_2\text{CH}_2\text{CO}$	$-\text{CH}_2-$ _n	CH_3	
Fatty acid-R1					$^3J_{\text{H}_2,\text{H}_3}$
$\delta^{13}\text{C}$	—	—	28.6	—	7.5 ± 0.1
$\delta^1\text{H}$	2.33	1.71	1.43–1.52	1.04	
Multiplicity	triplet	multiplet	multiplet	multiplet	
Fatty acid [†]					$^3J_{\text{H}_2,\text{H}_3}$
$\delta^{13}\text{C}$	—	—	≈ 29	—	7.4
$\delta^1\text{H}$	2.33	1.62	1.1–1.4	0.87–0.92	
Multiplicity	triplet	multiplet	multiplet	Triplet \times 3	

*In $^2\text{H}_2\text{O}$ at 40 °C, pH 7.5; accurate to ± 0.01 ppm. Chemical shifts were referenced to the internal HOD signal (4.800 ppm).

[†]Data taken from ref. 25.

proton signals was nearly identical to that determined by GC/MS composition analysis. Data obtained from matrix-assisted laser-desorption ionization (MALDI) mass spectrometry were consistent with a xylomannan structure, given that oligomers that varied by the mass of aldopentose and aldohexose monomers were observed (Fig. 5). The observation that the predominant hexose (Man) and pentose (Xyl) series share a common ion at 1618.23 m/z indicated that Man and Xyl comprise a core repeating structure.

The average molecular weight of the THF has not yet been established, but is bounded by the results of MALDI (1,000–2,400 Da) and centrifugal filtration experiments (<30 kDa). MALDI can substantially underestimate the molecular weight of polysaccharides because oligosaccharides suppress the ionization and desorption of larger saccharides (26). Thus, the MALDI

data may represent oligomers resulting from the degradation of the THF during storage.

THF Contains a β -Mannopyranose-(1 \rightarrow 4) β -Xylopyranose Backbone. We assigned the saccharide ^1H NMR signals for R1 using a combination of double quantum filtered correlation spectroscopy (DQF-COSY), TOCSY, heteronuclear single quantum coherence (HSQC), and HSQC-TOCSY 2D NMR methods (Fig. 6). ^1H and ^{13}C chemical shift assignments were consistent with those reported previously for Man and Xyl aldopyranosides when chemical shift patterns and signal multiplicities were taken into account (Table 2). The ^1H chemical shifts of H3 and H4 of Man were nearly identical, however, leading to the possibility that the ^1H signal assignments, and ^{13}C assignments derived from HSQC, might be reversed. The implications of this uncertainty are discussed below.

NMR analysis indicated that the Man and Xyl monosaccharide constituents are in the pyranosyl ring form (see preceding paragraph) configuration. The anomeric proton (H_1) proton were used to assign anomeric configuration. The value of $^3J_{\text{H}_1,\text{H}_2}$ (7.8 Hz) in the xylopyranose (Xylp) constituent was virtually identical to that reported in methyl β -D-xylopyranoside (27). The anomeric configuration of the Xylp residues was also confirmed with *endo* β -(1 \rightarrow 4)xylosidase treatment, which reduced the TH activity of a R1 sample from 0.6 ± 0.1 °C (\pm SD) to zero within 1 h of treatment at 22 °C.

In authentic methyl D-mannopyranosides, $^3J_{\text{H}_1,\text{H}_2}$ for the α and β anomers are 1.8 and 0.9 Hz, respectively (27). This coupling in the R1 THF was obscured by line broadening (≈ 3 Hz); when resolution enhancement was applied, the mannopyranose (Manp) H1 signal still appeared nearly symmetric and unsplit, suggesting a $^3J_{\text{H}_1,\text{H}_2}$ coupling <1 Hz, indicative of a β -configuration. To gain more information on the Manp anomeric configuration, we measured the one-bond $^1J_{\text{C}_1,\text{H}_1}$ coupling, which is very sensitive to anomeric configuration in Manp structures (27). The observed value of ≈ 160 Hz supported a β -configuration (27); however, broad signals and relatively poor signal/noise observed in the proton-coupled ^{13}C NMR spectrum led to uncertainty (± 10 Hz) in this measurement, allowing for a slight possibility that the Manp ring is in the α -configuration. ($^1J_{\text{C}_1,\text{H}_1}$ for α -Manp is 171.0 Hz). Additional support for the β -Manp configuration was obtained by noting that the chemical shift difference between the H2 and H3 signals (0.32 ppm) in the THF is much closer to the value observed in methyl β -D-mannopyranoside (0.35 ppm), than in methyl α -D-mannopyranoside (0.17 ppm) (26).

Carbon chemical shifts were used to establish the locations of O-glycosidic linkages (28). For the β -Manp and β -Xylp constit-

Fig. 4. Partial 800 MHz ^1H NMR and TOCSY spectra of R1 showing correlations among lipid signals. (A) ^1H NMR spectrum showing lipid signals that correspond to crosspeaks in (B). Numbers below the bracketed regions indicate relative signal areas. (B) Cross-peaks (connected by dashed lines) in the TOCSY spectrum indicate spin connectivities between CH_3 and different types of $-\text{CH}_2$ -protons in the fatty acid constituent of the R1 THF.

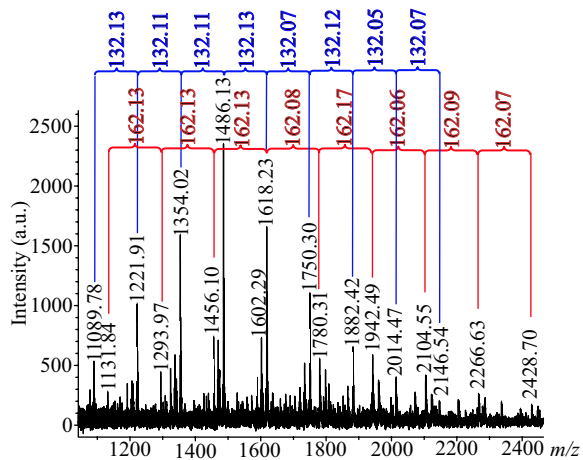


Fig. 5. MALDI-TOF mass spectrum of R1. Red and blue brackets indicate ions separated by either the mass of an aldohexose (180.06–18.01 [reducing end H_2O] = 162.05 Da) or aldopentose (150.05–18.01 [reducing end H_2O] = 132.04 Da), respectively.

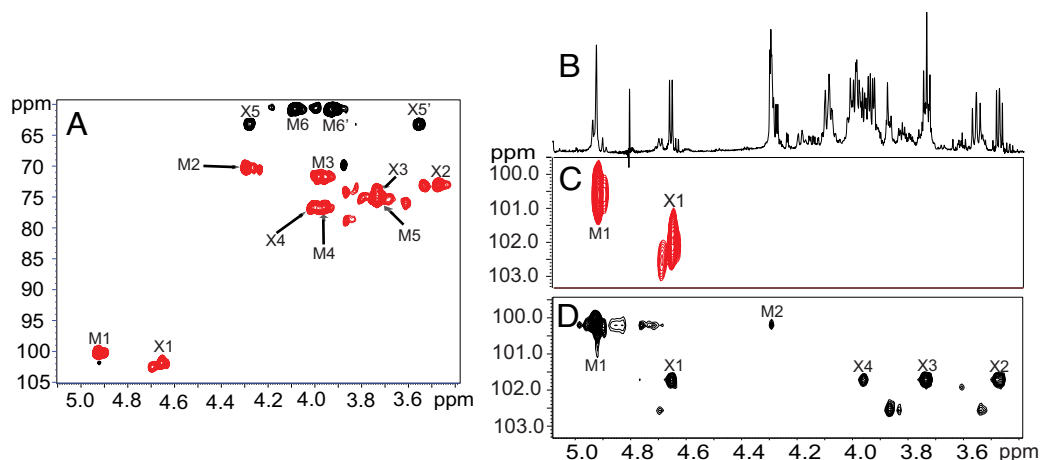


Fig. 6. Partial 2D ^1H NMR spectra of R1 at 800 MHz. (A) Partial HSQC spectrum showing ^1H - ^{13}C correlations for the saccharide ^1H signals shown in (B). Black contours correlate ^{13}C and methylene ($-\text{CH}_2-$) protons, and red contours correlate ^{13}C to methine ($-\text{CH}=\text{O}$) or methyl ($-\text{CH}_3$) protons. Crosspeak assignments for the Manp and Xylp constituents are shown as M1-M6' and X1-X5', respectively. (B) Partial 1D ^1H NMR spectrum showing saccharide signals observed for R1. (C) Expansion of the anomeric signals observed in the HSQC spectrum. (D) Partial HSQC-TOCSY spectrum showing proton signals in (B) that correlate with the anomeric signals observed in (C), allowing identification of most of the ring protons in Xylp, but only H2 in Manp because of the small $^3J_{\text{H1,H2}}$ and $^3J_{\text{H2,H3}}$ values in Man residues.

uents, the C4 chemical shifts were displaced downfield by 7–10 ppm relative to unsubstituted methyl pyranosides (Table 2), indicating that both saccharides are involved predominantly in β -(1 \rightarrow 4) linkages (Fig. 7). However, the saccharide sequence has not been established and may not strictly alternate between Manp and Xylp. For instance, there may be several tandem Manp residues followed by a series of Xylp residues. In addition, branching may also occur. The above-noted uncertainty in the assignment of the Manp H3 and H4 signals allows for the small possibility that Man may be involved in β -(1 \rightarrow 3) linkages. Interestingly, treatment of the THF with *endo* β -(1 \rightarrow 4)mannosidase did not affect TH activity.

Although the physiological role of THFs in freeze-tolerance is not well understood, THFs do appear to promote cold tolerance. Recrystallization inhibition and/or TH activity are known to increase in response to low temperature in freeze-tolerant insects (16, 17), other arthropods (20) and plants (6). For the centipede, *Lithobius forficatus*, experiments showed that THFs (i.e., AFPs) significantly increased cell survivorship under freezing conditions (29), although the mechanism remains unclear.

THFs are potent inhibitors of recrystallization; thus, one potential function is the prevention of damage associated with the recrystallization of extracellular ice. The observation that THFs were associated with the cell membrane in the centipede (29), as also appears to be the case for THFs from *U. ceramoides*, suggests that these molecules may prevent the spread of extracellular ice into the cytosol (intracellular freezing is typically thought to be lethal) and/or stabilize the plasma membrane at low temperature.

This study shows that a (lipo)xylomannan isolated from *U. ceramoides* is a highly active THF that is structurally distinct from all known AFPs and antifreeze glycoprotein (AFGPs) reported to date. In contrast to known AFGPs, which comprise 39% peptide by mass (1), THFs isolated from *U. ceramoides* contain little to no protein. In addition, the β -Manp-(1 \rightarrow 4)- β -Xylp backbone (Fig. 7) is unrelated to the saccharide component of fish AFGPs, which consists of β -D-galactosyl-(1 \rightarrow 3)- α -N-acetyl-D-galactosamine disaccharides (30). This ●●● xylomannan antifreeze may contribute to freeze tolerance by preventing recrystallization of extracellular ice, preventing intracellular freezing and/or stabilizing cellular membranes at low temperature.

Table 2. ^{13}C and ^1H chemical shifts (ppm) and ^1H - ^1H and ^{13}C - ^1H spin-couplings for saccharide signals in R1 and standard compounds

	Chemical shifts (ppm)						J -coupling (Hz)
	C1 (H1)	C2 (H2)	C3 (H3)	C4 (H4)	C5 (H5,H5')	C6 (H6,H6')	
Man: R1	100.2 [†] (4.92)	70.1 (4.30)	71.6 (3.98)	76.6 [†] (3.96)	75.1 (3.74)	60.6 (4.09, 3.93)	$^1J_{\text{C1,H1}} \approx 160$
methyl α -D-mannopyranoside ^{‡,§}	101.9 (4.854)	71.2 (4.024)	71.8 (3.851)	68.0 (3.739)	73.7 (3.70)	62.1 (3.991, 3.852)	$^1J_{\text{C1,H1}}$ 171.0
methyl β -D-mannopyranoside ^{‡,§}	101.3 (4.658)	70.6 (4.072)	73.3 (3.721)	67.1 (3.625)	76.6 (3.459)	61.4 (4.021, 3.825)	$^1J_{\text{C1,H1}}$ 159.5
Xyl: R1	101.7 [†] (4.66)	72.8 (3.48)	73.8 (3.73)	76.6 [†] (4.00)	63.0 (4.28, 3.55)		$^3J_{\text{H1,H2}}$ 7.8
methyl α -D-xylopyranoside ^{‡,§}	100.6 (4.868)	72.3	74.3	70.4	62.0		$^3J_{\text{H1,H2}}$ 3.6
methyl β -D-xylopyranoside ^{‡,§}	105.1 (4.415)	74.0 (3.345)	76.9 (3.533)	70.4 (3.713)	66.3 (4.064, 3.419)		$^3J_{\text{H1,H2}}$ 7.8

*In $^2\text{H}_2\text{O}$ at 40 °C, pH 7.5; accurate to ± 0.01 ppm. Chemical shifts were referenced to the internal HOD signal (4,800 ppm).

[†]Carbon resonances shifted 7–10 ppm downfield when compared with analogous carbons in the corresponding unsubstituted methyl glycoside, indicating involvement in an O-glycosidic linkage.

[‡]Data taken from ref. 35.

[§]Data taken from ref. 27.

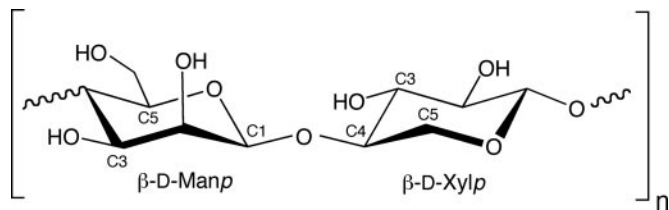


Fig. 7. Proposed disaccharide core structure comprising the THF isolated from *U. cerambyoides*.

Materials and Methods

Acclimation. *U. cerambyoides* were cold acclimated in darkness to the following schedule: 0 °C, 3 weeks; −1 °C, 5 days; −2 °C, 5 days; −3 °C, 7 days; −4 °C, 10 days; −5 °C, 10 days; −6 °C, 5 days; −7 °C, 5 days; and −8 °C, 2 weeks.

THF Extraction and Isolation. THFs were extracted from beetle whole bodies using a Bio-Rad ReadyPrep sequential extraction kit. The three buffer system permits the solubilization of increasingly hydrophobic biomolecules associated with plasma membrane (31). Extraction 1 and both washes were retained for ice affinity purification. Extractions 2 and 3 (tributyl phosphine omitted) and the corresponding washes were dialyzed (3,500 MW cut-off) against distilled water for 24 h. The osmolality of each sample was adjusted to \approx 200 mOsm with glycerol before ice affinity purification.

THFs selectively adsorb to ice and are incorporated into growing ice crystals, whereas other solutes are excluded. Thus, successive rounds of freezing permit the purification of THFs to homogeneity (21). The extractions and washes were aliquotted into 50-ml centrifuge tubes and placed in an alcohol bath set to −3.6 °C. Ice formation was initiated at the bottom of the tube with Fisherbrand spray freeze. After freezing overnight, the bottom 2.5 mm of each tube were excised with a razor blade and the unfrozen portion removed by centrifuging the tube at 2,000 rpm for 1 minute at 4 °C. The frozen fraction (>90%) was transferred to a new 50-ml centrifuge tube and thawed. The osmolality was readjusted to \approx 200 mOsm with glycerol and the sample was subjected to eight additional freeze–thaw cycles. On the ninth and final cycle, no glycerol was added to the sample, but the bath temperature was increased to −1.3 °C to remove residual glycerol from the sample. After the final cycle, the sample was dialyzed against distilled water for 48 h, lyophilized, and reconstituted in 20–50 μ l of MilliQ water.

Membrane Filtration. The R1 fraction was filtered through a Microcentrifugal filter device (Millipore; 30,000 MW cut-off) at 5,000 *g* for \approx 20 min. Before application of the sample to the filter cup, the filtration membrane was rinsed twice with distilled water. After the initial filtration, the retentate was rinsed twice, each time with 200 μ l of distilled water. All filtrate fractions were consolidated, lyophilized, and reconstituted before measurement of TH activity and subsequent NMR analysis. The retentate was resuspended in 20 μ l of distilled water to permit both the measurement of TH activity and analysis by polyacrylamide gel electrophoresis.

Thermal Hysteresis Measurements. TH was measured using a Clifton Nanoliter Osmometer (16).

NMR Spectroscopy. Lyophilized THF samples (R1 was filtered through 30,000 MWCO filter) were dissolved in 200 μ l of $^2\text{H}_2\text{O}$ containing \approx 20 mM sodium phosphate buffer, pH 7.5, and placed into a 5-mm symmetrical Shigemi NMR microtube susceptibility-matched to $^2\text{H}_2\text{O}$. Initial 1D ^1H NMR spectra were obtained on a Varian UNITYPlus 600 MHz FT-NMR spectrometer. Data acquisition parameters were as follows: 1,000 transients; 3 s recycle time; 313.15 K; −4 to 12 ppm spectral window. A line broadening function (0.2 Hz) was applied to free induction decays before Fourier transformation, yielding a final digital resolution of 0.07 Hz/pt. Spectra were referenced internally to the residual HOD signal (4,800 ppm).

Subsequent 1D and 2D spectra were obtained from the R1 sample (prepared as described above) on a Bruker Avance 800 MHz NMR spectrometer equipped with a 5-mm cryoprobe. The data acquisition parameters for 1D ^1H spectra were as follows: 80 transients; 3 s recycle time; 298.15 K or 313.15 K; spectral width 9615 Hz; digital resolution, 0.29 Hz/pt.

All two-dimensional NMR spectra were acquired in a phase-sensitive mode using the time proportional phase incrementation (32) for quadrature detection in the t1 dimension. TOCSY spectra were collected using isotropic mixing of times of 31 and 80.5 ms at 298.15 K. DFCOSY spectra were also collected

at 298.15 K. The data size for these spectra were 2048 (t2) \times 512 (t1). For all 2D spectra, data processing was performed on Bruker Biospin software and phase-shifted sine-squared window functions were applied before Fourier transformation. For TOCSY and DFCOSY spectra, final matrix sizes were 2048 \times 2048 real points with a final digital resolution of 4.7 Hz/pt in both F1 and F2. HSQC and HSQC-TOCSY spectra were collected at 313.15 K. Data size for HSQC and HSQC-TOCSY spectra were 2048 (t2) \times 256 (t1) and spectral widths were 22 kHz in the ^{13}C dimension and 9,600 Hz in the ^1H dimension. For the HSQC spectrum, the final matrix size was 2,048 \times 1,024 real points with a final digital resolution of 10.8 Hz/pt and 4.7 Hz/pt for F1 and F2, respectively. For the HSQC-TOCSY spectrum, the final matrix size was 2048 \times 512 real points, with a final digital resolution of 43 Hz/pt and 4.7 Hz/pt for F1 and F2, respectively.

$^{13}\text{C}\{^1\text{H}\}$ NMR spectra were also obtained on the Bruker 800 MHz spectrometer (200 MHz ^{13}C). The data acquisition parameters were as follows: 32,000 transients; 3 s recycle time; 313.15 K; 48,076 Hz spectral window. A line broadening function (3 Hz) was applied to free induction decays before Fourier transformation, yielding a final digital resolution of 0.73 Hz/pt. Conditions for obtaining the ^1H -coupled ^{13}C NMR spectrum were identical to those described above, with the exceptions that broadband ^1H -decoupling was not used during data acquisition and 56,000 transients were collected.

Amino Acid Chromatographic Analysis. A 20- μ g quantity of isolated THF from *U. cerambyoides* and an ice-purified blank (Tris buffer subjected to ice-affinity process) were sent to Texas A&M Protein Chemistry Laboratory for amino acid analysis. Four different samples were run for this assay: the ice-purified THF sample, the ice-purified blank, the assay blank, and human serum albumin as a control. Two internal standards norvaline (for primary amino acids) and sarcosine (for secondary amino acids) were added at the beginning of the assay to all samples to control for errors due to sample loss, injection variations and variability in preparing dilutions.

Each sample was mixed with the internal standards, divided into two aliquots and dried in glass tubes in a vacuum concentrator before vapor phase hydrolysis by 6N HCl at 150 °C for 1.5 h under an argon atmosphere. The samples were subsequently reconstituted in 0.4 N borate buffer to bring the pH to 10 for optimum derivitization and transferred to the AminoQuant autosampler for automated derivitization and loading. Amino acid analysis was performed using a HP AminoQuant II system. The system consists of an HP 1090 liquid chromatograph with an Hewlett-Packard Chemstation equipped with software that controls the LC and collects, analyzes and reports the data.

Sugar Composition Analysis. Sugar composition analysis was performed at the Complex Carbohydrate Research Center at the University of Georgia by combined gas chromatography/mass spectrometry (GC/MS) of the per-*O*-trimethylsilyl (TMS) derivatives of the monosaccharide methyl glycosides produced from the sample by acidic methanolysis (33, 34). Methyl glycosides were prepared from the isolated THF by methanolysis in 1 M HCl in methanol at 80 °C (18–22 h), followed by re-*N*-acetylation with pyridine and acetic anhydride in methanol (for detection of amino sugars). A 20- μ g quantity of inositol were added to the sample as an internal standard. The samples were then per-*O*-trimethylsilylated by treatment with Tri-Sil (Pierce) at 80 °C (0.5 h). GC/MS analysis of the TMS methyl glycosides was performed on an HP 6890 GC interfaced to a 5975b MSD, using an Alltech EC-1 fused silica capillary column (30 m \times 0.25 mm ID).

Enzymatic Hydrolysis Reactions. For each of the following enzymatic treatments, 1 μ l of THF solution (1–4 mg/ml) was diluted 1:1 with Pronase stock solution.

Pronase stock solution consisted of 2 mg/ml Pronase (a broad-spectrum protease) in Tris buffer, pH 7.5, containing 10 mM CaCl_2 . The reaction mixture was covered with mineral oil and incubated overnight at 37–40 °C. A 1:100 dilution of hemolymph from cold acclimatized *Dendroidea canadensis*, an AFP-producing beetle, was used as a positive control for the Pronase treatment.

B. *Endo* β -(1 \rightarrow 4) xylanase stock solution consisted of 2 mg/ml xylanase in 50 mM sodium citrate buffer, pH 5.0. The reaction mixture was held at 22 °C for 1 h.

C. *Endo* β -(1 \rightarrow 4) mannanase stock solution consisted of 1:10 dilution of ammonium sulfate enzyme suspension in 100 mM Mops, pH 7.0. Alternatively, the stock solution was prepared by dialysing the enzyme suspension overnight at 4 °C against 100 mM Mops, pH 7.0. The reaction mixture was covered with mineral oil and incubated overnight at 37 °C.

For the negative control in each of these treatments, the enzyme was omitted from the enzyme buffer added to the THF sample. The TH of all samples was measured immediately after addition of the enzyme and again after incubation.

MALDI-TOF Mass Spectrometry. The R1 sample was analyzed on a Bruker Autoflex III MALDI-TOF/TOF mass spectrometer in the negative polarity/reflector mode (detection range: 0–5,000 *m/z* with deflection up to 500 *m/z*). A 1- μ l quantity of diluted sample (\approx 4 μ g/ml) was added to 1 μ l of saturated 2,5-dihydroxybenzoic acid in 50/50 (v/v) acetonitrile/water.

ACKNOWLEDGMENTS. We thank Jaroslav Zajicek at the Lizzadro Magnetic Resonance Research Center at the University of Notre Dame for assistance

- DeVries AL, Komatsu SK, Feeney RE (1970) Chemical and physical properties of freezing point-depressing glycoproteins from Antarctic fishes. *J Biol Chem* 245:2901–2908.
- DeVries AL (1986) Antifreeze glycopeptides and peptides: Interactions with ice and water. *Methods Enzymol* 127:293–303.
- DeVries AL (2004) in *Life in the Cold: Evolution, Mechanisms, Adaptation and Application*, eds Barnes B, Carey H (Twelfth International Hibernation Symposium, Institute of Arctic Biology, Fairbanks), pp 307–315.
- Venketesh S, Dayananda C (2008) Properties, potentials, and prospects of antifreeze proteins. *Crit Rev Biotechnol* 28:57–82.
- Davies PL, Sykes BD (1997) Antifreeze proteins. *Curr Opin Struct Biol* 7:828–834.
- Griffith M, Yaish MW (2004) Antifreeze proteins in overwintering plants: A tale of two activities. *Trends Plants Sci* 9:399–405.
- Tomczak MM, Crowe JH (2002) in *Fish Antifreeze Proteins*, eds Ewart K, Hew C (World Scientific, New Jersey), pp 187–212.
- Hays LM, Feeney RE, Crowe LM, Crowe JH, Oliver AE (1996) Antifreeze glycoproteins inhibit leakage from liposomes during thermotropic phase transitions. *Proc Natl Acad Sci USA* 93:6835–6840.
- Duman JG, Bennett V, Sformo T, Hochstrasser R, Barnes BM (2004) Antifreeze proteins in Alaskan insects and spiders. *J Insect Physiol* 50:259–266.
- Urrutia ME, Duman JG, Knight CA (1992) Plant thermal hysteresis proteins. *Biochim Biophys Acta* 1121:199–206.
- Duman JG, Olsen TM (1993) Thermal hysteresis activity in bacteria, fungi and primitive plants. *Cryobiology* 30:322–328.
- Duman JG (2001) Antifreeze and ice nucleator proteins in terrestrial arthropods. *Annu Rev Physiol* 63:327–357.
- Graham LA, Davies PL (2005) Glycine-rich antifreeze proteins from snow fleas. *Science* 310:461.
- Hoshino T, et al. (2003) Antifreeze proteins from snow mold fungi. *Can J Bot* 81:1175–1181.
- Xu H, Griffith M, Patten CL, Glick BR (1998) Isolation and characterization of an antifreeze protein with ice nucleation activity from the plant growth promoting rhizobacterium *Pseudomonas putida* GR12–2. *Can J Microbiol* 44:64–73.
- Walters KR, Jr., Sformo T, Barnes BM, Duman JG (2009) Freeze tolerance in an Arctic Alaska stonefly. *J Exp Biol* 212:305–312.
- Wharton DA, Pow B, Kristensen M, Ramlöv H, Marshall CJ (2009) Ice-active proteins and cryoprotectants from the New Zealand alpine cockroach *Celatoblatta quinque maculata*. *J Insect Physiol* 55:27–31.
- Davies PL, Ewart KV, Fletcher GL (1993) *Fish Biochemistry and Molecular Biology*, vol 2, eds Mommsen T, Hochachka P (Elsevier, Amsterdam) pp 279–291.
- Miller LK (1982) Cold-hardiness strategies of some adult and immature insects overwintering in interior Alaska. *Comp Biochem Physiol* 73A:595–604.
- Tursman D, Duman JG, Knight CA (1994) Freeze tolerance adaptations in the centipede, *Lithobius forficatus*. *J Exp Zool* 268:347–353.
- Kuiper MJ, Lankin C, Gauthier SY, Walker VK, Davies PL (2003) Purification of anti-freeze proteins by adsorption to ice. *Biochem Biophys Res Comm* 300:645–648.
- Berggren K, et al. (2000) Background-free, high sensitivity staining of proteins in one- and two-dimensional sodium dodecyl sulfate-polyacrylamide gels using a luminescent ruthenium complex. *Electrophoresis* 21:2509–2521.
- Li N, Zachariassen KE (2007) Cold hardiness of insects distributed in the area of Siberian Cold Pole. *J Comp Phys A* 146:5156–5157.
- Wilson SL, Kelley DL, Walker VK (2006) Ice-active characteristics of soil bacteria selected by ice-affinity. *Environ Microbiol* 8:1816–1824.
- Huang Y, Anderson R (1989) Structure of a novel glucosamine containing phosphoglycolipid from *Deinococcus radiodurans*. *J Biol Chem* 264:18667–18672.
- Garrozzo D, Impallomeni G, Spina E, Sturiale L (1995) Matrix assisted laser ionization/desorption of polysaccharides. *Rapid Commun Mass Spectrom* 9:937–941.
- Podlasek CA, Wu J, Stripe WA, Bondo PB, Serianni AS (1995) ^{13}C -enriched methyl aldopyranosides: Structural interpretations of ^{13}C - ^1H spin-coupling constants and ^1H chemical shifts. *J Am Chem Soc* 117:8635–8644.
- Prohaska R, Koerner T, Jr., Armitage IM, Furthmayr H (1981) Chemical and carbon-13 nuclear magnetic resonance studies of the blood group M and N active sialoglycopeptides from human glycoporphin A. *J Biol Chem* 256:5781–5791.
- Tursman D, Duman JG (1995) Cryoprotective effects of thermal hysteresis protein on survivorship of frozen gut cells from the freeze tolerant centipede, *Lithobius forficatus*. *J Exp Zool* 272:249–257.
- Shier WT, Lin Y, DeVries AL (1975) Structure of carbohydrate of antifreeze glycoproteins from an Antarctic fish. *FEBS Lett* 54:135–138.
- Molloy MP, et al. (1998) Extraction of membrane proteins by differential solubilization for separation using two-dimensional gel electrophoresis. *Electrophoresis* 19:837–844.
- Marion D, Wüthrich K (1983) Application of phase sensitive two-dimensional correlated spectroscopy (COSY) for measurement of ^1H - ^1H spin-spin coupling constants in proteins. *Biochem Biophys Res Commun* 113:967–974.
- Merkle RK, Poppe I (1994) Carbohydrate composition analysis of glycoconjugates by gas-liquid chromatography/mass spectrometry. *Methods Enzymol* 230:1–15.
- York WS, Darvill AG, McNeil M, Stevenson TT, Albersheim P (1985) Isolation and characterization of plant cell walls and cell wall components. *Methods Enzymol* 118:3–40.
- Bock K, Pedersen C ^{13}C NMR spectroscopy of monosaccharides (1983) *Adv Carbohydr Chem Biochem* 41:27–66.